Dynamic tensile measurements for $Pt_{60}Ni_{15}P_{25}$ below the calorimetric glass transition temperature

1999 J. Phys.: Condens. Matter 11 3029

(http://iopscience.iop.org/0953-8984/11/15/009)

J. Phys.: Condens. Matter **11** (1999) 3029–3042. Printed in the UK PII: S0953-8984(99)00435-X

Dynamic tensile measurements for $Pt_{60}Ni_{15}P_{25}$ below the calorimetric glass transition temperature

D N Perera and A P Tsai

Aperiodic Solids Research Team, National Research Institute for Metals (NRIM), 1-2-1 Sengen, Tsukuba, Ibaraki 305-0047, Japan

Received 30 December 1998

Abstract. Dynamic tensile measurements have been carried out on a ternary metallic alloy, $Pt_{60}Ni_{15}P_{25}$, below and close to the calorimetric glass transition temperature. The storage and loss tensile moduli, as well as the complex and dynamic tensile viscosity, are found to obey the time–temperature superposition principle in this temperature range. Structural relaxation times were measured from the position of the maximum in the loss modulus and from the limiting low-frequency value of the complex viscosity and its real component. The three quantities display Arrhenius temperature dependences with similar activation energies and indicate that the metallic alloy has an intermediate fragility strength in the general classification scheme for glass-forming liquids. The master curves obtained by scaling the measured dynamic properties by the appropriate relaxation time reflect a very broad distribution of microscopic relaxation times. A discrete spectrum of relaxation frequencies has been calculated from the master curve for the storage modulus assuming a superposition of intrinsic exponential responses. The resulting distribution is broad and skewed towards high frequencies, a characteristic feature of heterogeneous relaxation. It is found that the high-frequency end of the relaxation spectrum controls the amplitude, whereas the low-frequency end determines the width of the overall macroscopic response. The results presented here indicate a very high degree of dynamic heterogeneity in the tensile relaxation process for supercooled $Pt_{60}Ni_{15}P_{25}$.

1. Introduction

There is now an extensive body of experimental data to demonstrate that a wide range of chemically disparate materials can be quenched below the freezing temperature T_f into a stable amorphous state which is devoid of long-range ordering. In each of these materials, the viscosity rises very rapidly below T_f until, eventually, viscous flow ceases on the timescale of the experimental probe within a narrow temperature interval centred around the glass transition temperature T_g.

In order to achieve some semblance of order among the vast range of glass-forming substances, a simple scheme was developed by Laughlin and Uhlmann [1], and later popularized by Angell [2], for classifying the materials according to the temperature dependence of the viscosity or some other structural relaxation time. A glass former with an Arrhenius temperature dependence of the viscosity or a relaxation time between T_f and T_g is referred to as a strong liquid and one showing considerable deviation from Arrhenius behaviour is called a fragile liquid.

0953-8984/99/153029+14$19.50

The magnitude of the departure from Arrhenius behaviour is quantified by a fragility parameter m defined as [3, 4]

$$m = \left.\frac{\mathrm{d}\log_{10}\tau(T)}{\mathrm{d}T_g/T}\right|_{T=T_g} \tag{1}$$

where $\tau(T)$ is a characteristic temperature-dependent relaxation time. The lower limit of the fragility parameter corresponding to strong liquids is $\approx$16, whereas extremely fragile liquids have $m \geqslant 100$. Böhmer and co-workers have compiled the fragility parameters for approximately 70 glass formers consisting of simple and complex covalent molecular liquids, polymers, ionic melts, oxides and alcohols. However, no data on metallic alloys have been included in this compilation.

Methods of preparing thin films and bulk metallic glasses are now fairly routine [5]. Most of these metallic glasses consist of ternary and quarternary alloys. Among the broad classes of glass formers, metallic alloys possess one of the simplest microstructures and, thus, present an ideal realistic system for which to compare the trends and predictions derived from theoretical models of the glass transition, such as mode-coupling theory [6], and from computer simulations of spherical particles. However, the main body of theoreticians in the field of supercooled condensed matter still lack a greater degree of awareness of the research conducted by metallurgists in this area.

In this paper, we present experimental results for a ternary metallic alloy, $Pt_{60}Ni_{15}P_{25}$, which indicate that it has some bulk-averaged characteristics which are similar to those of several supercooled polymeric and molecular organic liquids. We report dynamic measurements of the tensile storage and loss moduli of thin ribbons of $Pt_{60}Ni_{15}P_{25}$ near and below its glass transition temperature T_g. The tensile complex viscosity and its real component (the dynamic viscosity) were also calculated from these results. From the frequency dependences of the complex and dynamic viscosities, constant limiting low-frequency viscosities which are proportional to structural relaxation times can be determined. The frequency of maximum loss in the tensile modulus also provides another relaxation time. The results on the temperature dependences of these relaxation times are an important addition to this field. Such results for various glass-forming systems are fervently sought since the study of the rapid increase in timescales as T_g is approached lies at the heart of the research into supercooled liquids and glasses.

From the temperature variation of the relaxation times for $Pt_{60}Ni_{15}P_{25}$, we have also calculated the fragility index m in order to supplement the compilation of such data in reference [4]. We find that the amorphous alloy is an intermediate glass, lying between the strong and fragile extremes in the classification scheme described earlier. It is also found that a high degree of dynamic heterogeneity dominates the relaxation in this glassy alloy.

2. Experimental method

Amorphous ribbons of $Pt_{60}Ni_{15}P_{25}$ (concentrations in at.%) were prepared by rapid quenching of the melt using a single-roller melt-spinning technique [7]. The ribbons have thicknesses of 0.024 ± 0.004 mm and widths of 1.02 ± 0.03 mm. All of the samples used in this study came from this single production batch. The glass transition region can be detected from differential scanning calorimetry (DSC) scans as an endothermic change in the heat flow curve during heating of the metallic glass from low temperatures. We define T_g as the temperature corresponding to the mid-point of the endothermic transition. The calorimetric T_g will be denoted as T_g^c. At a scanning rate of 20 K min^{-1}, $T_g^c = 485 \pm 2$ K. The crystallization (exothermic) peak maximum at this heating rate occurs at $T_x = 550$ K with an onset at $\approx$543 K.

Thus, the supercooled liquid region extends over ≈55 K. The glass transition temperature still lies within the range given above when the heating rate is dropped to 10 and 5 K min^{-1}.

Tensile dynamic measurements were carried out using a Rheometrics Solids Analyzer (RSA-II) in which the sample is coupled between an actuator and a transducer. The actuator imposes an oscillatory deformation upon the material, whereas the transducer measures the resultant force generated by the sample deformation. The electrical current required to maintain the axial position of the transducer is proportional to this force. Sample displacement is determined from measured actuator and transducer axial displacements. The angular frequency range of the RSA-II is $\omega = 10^{-3}$ to 10^{2} rad s^{-1}. In the present study, a sinusoidal strain with a constant amplitude of 4.5×10^{-4}, which lies within the linear viscoelastic region, was employed.

Measurements of the dynamic tensile storage ($E'(\omega)$) and loss ($E''(\omega)$) moduli were made just below T_g^c from 460 K to 480 K with a step of 5 K. At $T \geqslant T_g^c$, the samples become too 'soft' in the sense that they rapidly extend to the machine's extension limit (4 mm) before the measurement process is complete. At each measurement temperature, the samples were equilibrated for at least one hour. This annealing step is required to eliminate any fast initial relaxation process due to the change in temperature and for the system to reach internal metastable equilibrium. The annealing process is necessary to obtain reproducible results when the samples are changed. All relaxation curves shown in this study have been averaged over at least ten individual measurements using different samples.

3. Experimental results

3.1. Tensile moduli

The tensile moduli $E'(\omega)$ and $E''(\omega)$ are shown in figure 1 for the range of temperatures studied. Observe the rapid change in relaxation times over the 20 K interval directly below T_g^c. This change is quantified by measuring the position ω_{max} of the peak maximum in $E''(\omega)$ for $T = 465$ K to 480 K which falls within the experimental frequency window. The temperature dependence of ω_{max} is plotted in an Arrhenius plot in figure 2. A straight line can be fitted through the four data points with an activation energy of $E_a = 625 \pm 10$ kJ mol^{-1} (149 ± 2 kcal mol^{-1}) and a prefactor of $\omega_0 = 1.81 \times 10^{68}$ rad s^{-1}. From this Arrhenius equation, ω_{max} for the lowest temperature at $T = 460$ K was calculated and is also shown in figure 2. As can be seen, the relaxation time changes by approximately three orders of magnitude over the narrow temperature interval.

Since the measurement of ω_{max} lies very close to T_g^c, we expect the Arrhenius equation to apply at T_g^c. Hence, it is possible to calculate the so-called fragility parameter [4] defined in equation (1). For the $Pt_{60}Ni_{15}P_{25}$ alloy, $m = E_a/(RT_g^c \ln 10) = 67.3$, where R is the gas constant. As stated earlier, strong liquids correspond to $m < 30$ whereas extremely fragile liquids have $m \geqslant 100$. Thus, the metallic alloy lies somewhere intermediate between the two extremes and has a fragility strength that is similar to several organic liquids such as dibutylphthalate, tri-α-naphthylbenzene, 1, 3-butanediol and 1, 4-*cis*-polyisoprene which have m in the range of 60 to 70 [4].

3.1.1. Time–temperature superposition. Both $E'(\omega)$ and $E''(\omega)$ fall onto master curves when plotted against frequency scaled by $\omega_{max}(T)$ as shown in figures 3 and 4 respectively. The shifted data points now extend over approximately eight orders of magnitude. There is a systematic drop in the storage modulus with increasing temperature on the high-frequency side, $\omega/\omega_{max} > 1$. This decrease is more clearly evident for the loss modulus. We note that

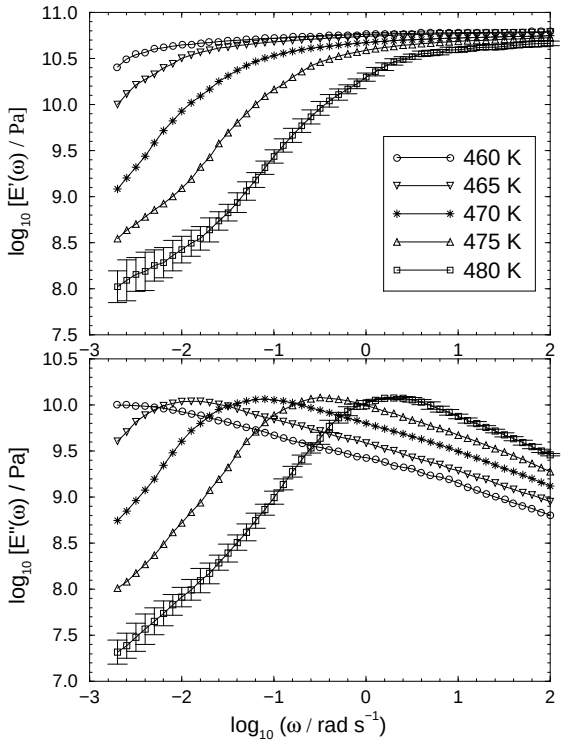

Figure 1. The tensile storage ($E'(\omega)$) and loss ($E''(\omega)$) moduli for $Pt_{60}Ni_{15}P_{25}$ below $T_g^c = 485 \pm 2$ K from $T = 460$ K to 480 K. The precision of the results is shown for the highest temperature $T = 480$ K where the error bars denote $+/-$ the standard deviation.

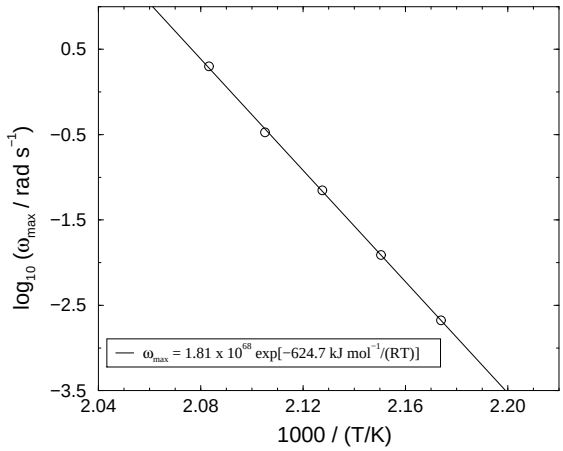

Figure 2. The temperature dependence of the position ω_{max} of the peak maximum in $E''(\omega)$. The solid line is a linear regression through the four experimental data points from $T = 465$ to 480 K. The point at $T = 460$ K or $1000/T = 2.174$ K^{-1} was calculated from this linear relation.

a common curve can also be obtained if any one of the $E'(\omega)$ (or $E''(\omega)$) curves are fixed and the remaining temperature curves are shifted to superpose onto the selected curve, i.e. the

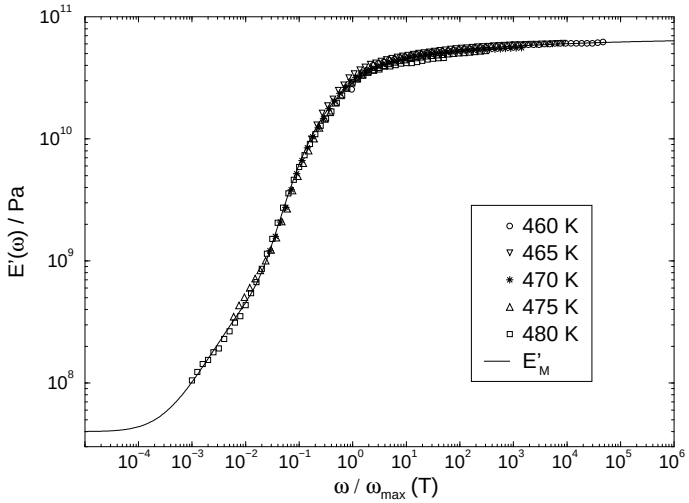

Figure 3. The result of plotting the storage modulus against angular frequency scaled by $\omega_{\max}(T)$. The solid curve is the fit given by equation (3).

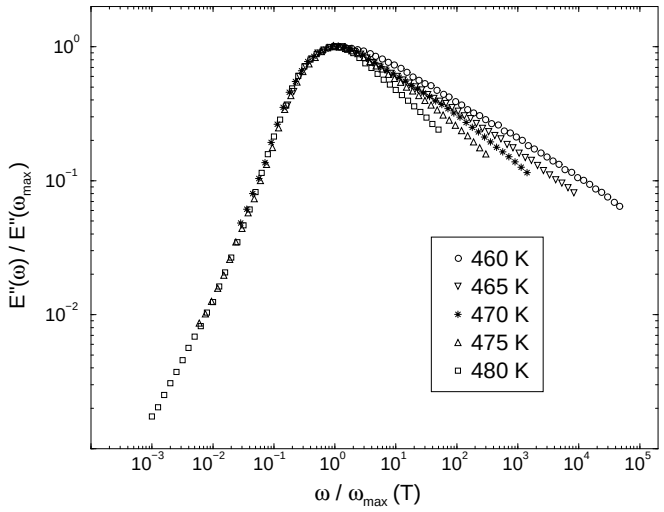

Figure 4. The result of plotting the loss modulus against angular frequency scaled by $\omega_{\max}(T)$.

time–temperature superposition principle applies. This means that the common curves shown in figures 3 and 4, at least on the low-frequency side ($\omega/\omega_{\max} < 1$), are the relaxation curves for the temperature corresponding to $\omega_{\max} = 1$ rad s^{-1}, which according to figure 2 occurs at $T = 478$ K.

It is now well documented that relaxation functions of many supercooled liquids can be reasonably well described by the empirical Kohlrausch–Williams–Watts (KWW) or stretched exponential function [8]:

$$\phi(t) = A \exp\left[-\left(\frac{t}{\tau}\right)^{\beta}\right] \qquad 0 < \beta \leqslant 1 \tag{2}$$

where $\phi(t)$ is a relaxation function, A is an adjustable parameter, τ is a characteristic relaxation time and β is a measure of the departure from exponential relaxation ($\beta = 1$). We have attempted to fit the master curve for the storage modulus with the above relation. It is obvious from the shape of this curve in figure 3 that a smaller stretching parameter β is required at low frequencies ($\omega < 0.03\omega_{max}$) than at higher frequencies. A superposition of two such equations which provides a reasonably good fit to the master curve is given by

$$E'_M\left(\frac{\omega}{\omega_{max}}\right) = 4.6 \times 10^{10} \exp\left[-0.60\left(\frac{\omega_{max}}{\omega}\right)^{0.58}\right] + 2.1 \times 10^{10} \exp\left[-1.8\left(\frac{\omega_{max}}{\omega}\right)^{0.17}\right] + E_0 \tag{3}$$

where E_0, the discrete contribution to the spectrum for viscoelastic solids as $\omega \to 0$, was chosen to be 4.0×10^7 Pa from the trend of the decay of the experimental data. The master curve fit $E'_M(\omega/\omega_{max})$ is also shown in figure 3. The first term in the above equation fits the shape of the initial part of the relaxation, while the second term fits the tail ($\omega < 0.03\omega_{max}$). Young's modulus $E_\infty = E'(\omega \to \infty)$, estimated from $E'_M(\omega/\omega_{max})$, is 6.63×10^{10} Pa.

In reference [4] a correlation between the fragility index and the stretching parameter given by

$$m \approx 250 - 320\beta \tag{4}$$

has been found to apply for a wide variety of amorphous materials. Inserting $\beta = 0.58$ from equation (3) into equation (4) gives $m = 64.4$ in agreement with the result obtained from $\omega_{max}(T)$. Using $\beta = 0.17$ gives $m = 196$ which indicates extreme fragility. We note, however, that the data for the low-frequency end of the spectrum are less precise than those for the higher-frequency end as shown for example in figure 1 for $T = 480$ K. The organic liquids mentioned previously which have a similar fragility strength to $Pt_{60}Ni_{15}P_{25}$ have β in the range 0.50 to 0.60 [4].

3.1.2. The spectrum of relaxation frequencies. The main kinetic feature of relaxation in many supercooled liquids is dynamic heterogeneity, characterized by both a broad distribution of local relaxation times and a non-uniform spatial distribution of such times [9–13]. In order to obtain an estimate of the spread of relaxation times for the supercooled $Pt_{60}Ni_{15}P_{25}$ alloy, we have calculated an approximate distribution of relaxation frequencies for the master curve of the storage modulus by assuming a superposition of exponentially decaying microscopic processes, that is we have approximated E'_M by a sum of exponentials:

$$E'_M\left(\frac{\omega}{\omega_{max}}\right) = \sum_{i=1}^{N} H_i \exp\left[-\frac{\omega_i}{\omega}\right] \tag{5}$$

where H_i and ω_i are the amplitude and relaxation frequency of the individual intrinsic responses. The assumption inherent in equation (5) is reasonable considering the results of recent multi-dimensional nuclear magnetic resonance [11, 12] and time-dependent solvation spectroscopy [11, 13] experiments which have demonstrated that the non-exponential primary relaxation in a variety of supercooled molecular and polymeric organic liquids is due to a broad distribution of singly decaying intrinsic processes, each with its own characteristic time constant. This form of relaxation is often referred to as the heterogeneous limit [11], as opposed to the homogeneous extreme where the individual microscopic processes are proportional to the macroscopic response function and the relaxation spectrum is represented by a Dirac delta distribution.

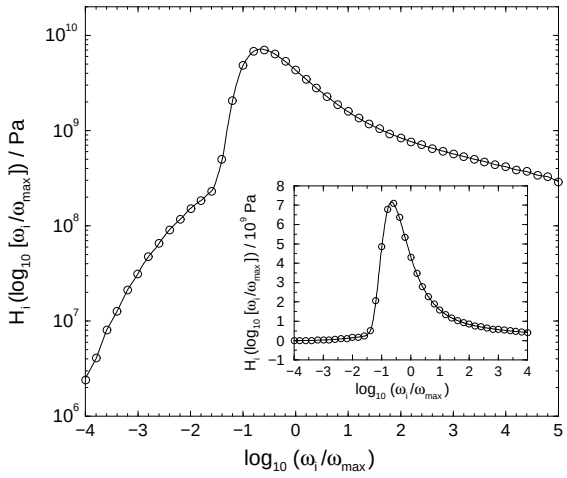

Figure 5. The frequency probability density for the master curve $E'_M(\omega/\omega_{\max})$ shown in figure 3. The inset shows the same distribution on a linear scale for the ordinate.

Using $N = 101$ and $\log_{10}\omega_i$ equally spaced in the interval $[-10, 10]$, equation (5) was solved using the general linear least-squares algorithm provided in *Numerical Recipes* [14]. The resulting probability density of relaxation frequencies $H_i(\log_{10}\omega_i)$ is shown in figure 5. We find that the truncated relaxation spectrum in the range $\log_{10}\omega_i \in [-4, 4]$ is already sufficient to fit E'_M with a precision >99.9%. The probability density in figure 5 has the general characteristics observed for several supercooled organic liquids mentioned in references [11–13], i.e. a very broad asymmetrical distribution which drops rapidly on the low-frequency side of the maximum and declines more gently on the high-frequency side. These features are associated with a high degree of dynamic heterogeneity. One difference between the distribution for $Pt_{60}Ni_{15}P_{25}$ and those for the aforementioned organic liquids is the development of a 'step' and slower decay on the low-frequency side of the main peak starting at $\log_{10}(\omega_i/\omega_{\max}) \approx -1.6$. The development of this broader distribution in the relaxation spectrum coincides with the change in the stretching parameter β from 0.58 to 0.17 in the decay of E'_M.

We have attempted to analyse the contribution of different sections of the relaxation spectrum to the overall response function E'_M. This was done by first fixing the lower limit of the summation in equation (5) at $\Omega_{\min} = \log_{10}(\omega_i/\omega_{\max}) = -10$ and selectively truncating the upper limit $\Omega_{\max} = \log_{10}(\omega_i/\omega_{\max})$ at decreasing frequencies. The result of varying $\Omega_{\max}$ is shown in figure 6(a). The main consequence of not including the high-frequency end of the probability density in the calculation of the macroscopic response is to reduce the height of the overall curve $E'(\omega/\omega_{\max})$. There is an especially large drop in the amplitude in going from $\Omega_{\max} = -1$ to -2. When $\Omega_{\max} = -2$, only the secondary-step portion of the low-frequency side of the relaxation spectrum is contributing to the overall response and, hence, the resulting relaxation curve has a stretching parameter $\beta = 0.17$ as can be seen in figure 6(a).

Next $\Omega_{\max}$ was fixed at 10 and $\Omega_{\min}$ was successively increased in order to investigate the consequence of removing the low-frequency constants from the macroscopic response. The resulting relaxation curves are shown in figure 6(b). Note that when $\Omega_{\min} = -4$, the relaxation curve is not distinguishable from E'_M on the scale shown in figure 6(b). However, on going from $\Omega_{\min} = -4$ to -3, the tail of the overall relaxation becomes less broad. Further increase of $\Omega_{\min}$ results in a gradual increase of the stretching parameter β for the low-frequency side

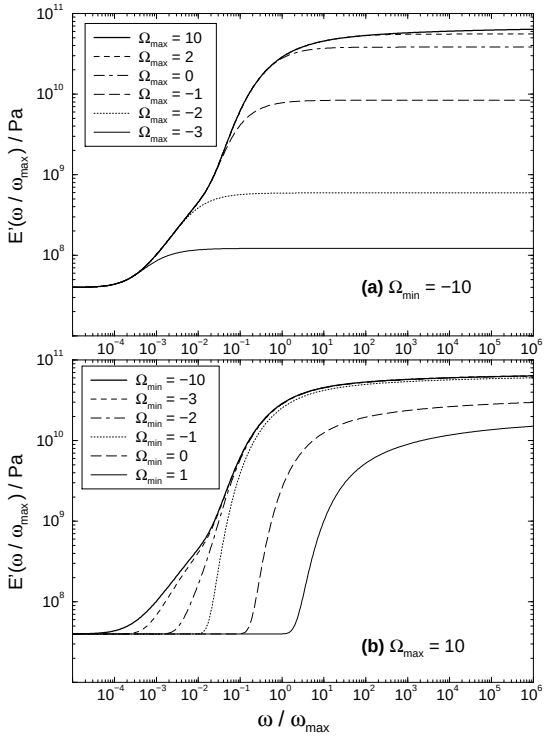

Figure 6. The macroscopic relaxation curves for the storage modulus obtained by truncating the relaxation spectrum shown in figure 5 on (a) the high-frequency side and (b) the low-frequency side as described in section 3.1.2. The thick solid curves in (a) and (b) are the master curve fits E'_M shown in figure 3.

of the relaxation to $\beta = 0.58$ at $\Omega_{\min} = -1$. For $\Omega_{\min} > -1$ the value of β does not change from 0.58 but the amplitude of the macroscopic function decreases as increasingly more of the high-frequency constants are not included in equation (5).

In summary, the high-frequency side of the frequency probability density controls the amplitude of the overall response, whereas the low-frequency side determines the width of the tail of this macroscopic relaxation function.

3.2. The loss tangent

A measure of the ratio of energy loss to energy stored in a cyclic deformation is provided by the loss tangent,

$$\tan\delta = \frac{E''(\omega)}{E'(\omega)}. \tag{6}$$

The frequency dependence of $\tan\delta$ is shown in figure 7. As can be seen, the main peak in $\tan\delta$, corresponding to a region of maximum loss, moves towards higher frequencies as the temperature increases. For the lowest temperature of 460 K, this maximum does not lie within the experimental frequency window. A shoulder or secondary maximum is also clearly observable on the lower-frequency side within our frequency window for the higher temperatures of $T = 475$ K and 480 K. The height of this secondary peak is lower than that of the main loss peak. Such characteristics are found to be similar in shape to the $\tan\delta$ curves for

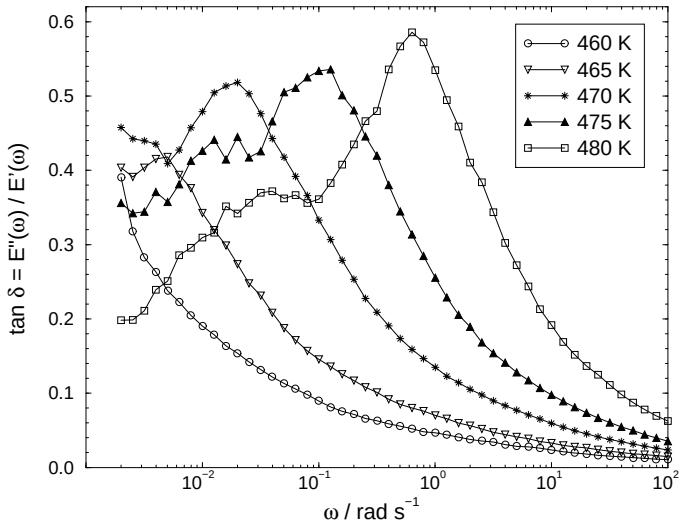

Figure 7. The $\tan\delta = E''(\omega)/E'(\omega)$ curves for the temperatures investigated. Observe the existence of a secondary maximum on the low-frequency side of the main peak for the two highest temperatures.

lightly cross-linked amorphous polymers [15]. For the polymers, the subsidiary maximum at the lower frequency is attributed to losses incurred in entanglement slippages. For the metallic alloy, we do not know what gives rise to the secondary maximum, except to note that it signals a change in the dissipative mechanism from that at higher frequencies. It is possible that the shorter loss peak, due to its position at low frequencies, is associated with viscous cooperative rearrangements of large atomic regions.

3.3. Complex tensile viscosity

The frequency dependence of the complex tensile viscosity $\eta^*(\omega)$ is shown in figure 8 for all temperatures investigated. At low ω, $\eta^*(\omega)$ reaches a limiting constant value $\eta^*(0)$. As ω increases, there is a gradual drop in the viscosity until it becomes inversely proportional to ω at high frequencies as shown by the solid line in figure 8. The frequency at which the viscosity begins to decrease from $\eta^*(0)$ increases with temperature.

The shape of the $\eta^*(\omega)$ curves in figure 8 is the same as the variation of the shear viscosity η_s with increasing shear rate $\dot{\gamma}$ in polymers [16] and metallic alloys [17]. The constant low $\dot{\gamma}$-value of η_s is called the Newtonian viscosity and the high-$\dot{\gamma}$ region in which η_s drops with increasing $\dot{\gamma}$ is referred to as the non-Newtonian regime. Experimental data for polymers [16] indicate that η_s at high shear rates has a power-law dependence on $\dot{\gamma}$, i.e. $\eta_s \propto \dot{\gamma}^{-n}$ with $n < 1$ and commonly $n \approx 0.8$. It has recently been found that $n = 1$ for a quarternary metallic alloy, $Pd_{40}Ni_{10}Cu_{30}P_{20}$, near the glass transition [17]. Our results for $Pt_{60}Ni_{15}P_{25}$ at high frequencies where $\eta^*(\omega) \propto \omega^{-1}$ are in accord with the behaviour for the quarternary alloy. It would be interesting to examine whether $n = 1$ for all glass-forming metallic alloys—that is, whether these materials form a special limiting case due to their simpler microstructure.

Theories of non-Newtonian flow in polymers have proposed that the decrease in apparent viscosity with increasing shear rate is due to a decrease in the concentration of intermolecular entanglements [18]. In the Newtonian regime a steady state is achieved between the formation

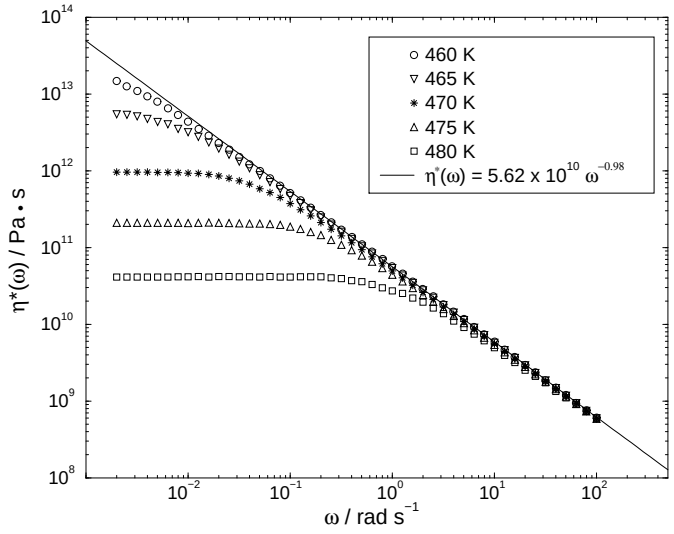

Figure 8. The frequency dependence of the complex tensile viscosity $\eta^*(\omega)$ for $T = 460$ K to 480 K. At high frequencies $\eta^*(\omega)$ becomes inversely proportional to ω as shown by the solid line.

and break-up of entanglements. Above a critical shear rate, however, the transit time during which molecular segments are close enough to become entangled as they shear past each other becomes shorter than the time required to form the entanglement and, as a consequence, the apparent viscosity drops. In the case of metallic alloys, computer simulations of Lennard-Jones particles [19] suggest that for a given temperature, there is a critical shear rate above which structural reorganization is dominated by the velocity profile imposed by the shearing action. This results in the formation of layers in the liquid along the direction of shear which slide past one another during the shearing process, thus facilitating flow and reducing the apparent viscosity. At higher temperatures, due to the greater degree of kinetic motion in the system, a larger shear rate is required to force preferential ordering along the lines of shear.

In figure 9 is plotted the temperature dependence of $\eta^*(0)$ for $Pt_{60}Ni_{15}P_{25}$ from $T = 465$ K to 480 K at which temperatures this limiting value can be determined from within the experimental window. A linear regression through the four data points gives an activation energy of $E_a = 600 \pm 10$ kJ mol^{-1} (143 ± 2 kcal mol^{-1}) and a prefactor of 2.0×10^{-55} Pa s. This activation energy is approximately equal to the activation energy for the position, ω_{max}, of the tensile loss peaks discussed in section 3.1. From the above Arrhenius relation, $\eta^*(0)$ for $T = 460$ K was calculated and is also shown in figure 9. The viscosity $\eta^*(0)$ changes by approximately three orders of magnitude over the 20 K interval below T_g^c in accordance with $\omega_{max}(T)$. We also plot in figure 9 the limiting zero-frequency value $\eta'(0)$ of the real component $\eta'(\omega)$ of $\eta^*(\omega)$. As can be seen, there is an approximately systematic decrease in $\eta'(0)$ compared to $\eta^*(0)$ at all temperatures investigated. The temperature dependence of $\eta'(0)$ can also be fitted with an Arrhenius relation with an activation energy of 610 ± 10 kJ mol^{-1} and a prefactor of 5.9×10^{-57} Pa s.

The fragility parameter m of equation (1) at T_g^c, calculated using the temperature dependence of $\eta^*(0)$, is 64.6. This value is close to the value of 67.3 determined from the Arrhenius relation for ω_{max} and approximately equal to the fragility parameter ($m = 64.4$) calculated from equation (4) using the stretching parameter $\beta = 0.58$ from equation (3). The fragility parameter calculated using the activation energy for $\eta'(0)$ is 65.7 which is also

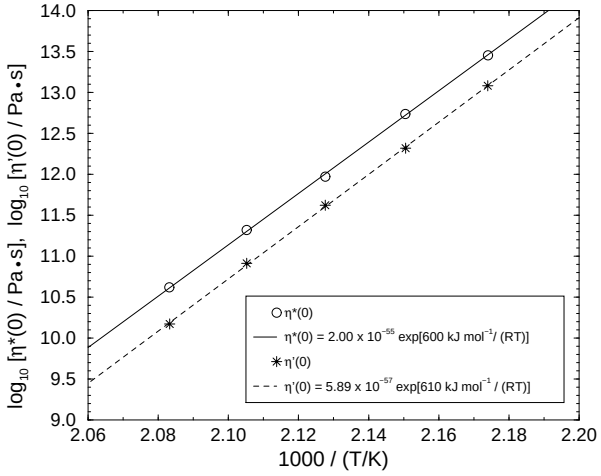

Figure 9. An Arrhenius plot of the constant limiting low-frequency value, $\eta^*(0)$ and $\eta'(0)$, of the complex tensile viscosity and its real component respectively. The solid and dashed lines are linear regressions through the experimental data points from $T = 465$ to 480 K only. The points for $T = 460$ K were calculated from the respective linear relations.

in agreement with the above values. If instead the glass transition temperature T_g^v is taken to be the temperature at which the viscosity is 10^{12} Pa s, then the Arrhenius relation for $\eta^*(0)$ gives $T_g^v = 470$ K and $m = 66.7$, and the corresponding values from the temperature dependence of $\eta'(0)$ are $T_g^v = 467$ K and $m = 68.2$. In summary, the fragility parameter for $Pt_{60}Ni_{15}P_{25}$ calculated from our results is $m = 66 \pm 3$. Previously, Chen [20] estimated the temperature dependence of the viscosity of $Pt_{60}Ni_{15}P_{25}$ near T_g^c by measuring rates of thermal transformation. For a heating rate of 20 K min^{-1}, $T_g^c = 482$ K for his sample. The fragility index calculated from his data at this temperature is $m = 50$ which is lower than our estimate. However, at T_g^v (defined as above), which occurs at 463 K according to his data, the value of m calculated from his parameters is 64 which is in much better agreement with our result.

Just as in the case of the shear viscosity $\eta_s(\dot{\gamma})$ which falls onto a master curve when $\dot{\gamma}$ is scaled by the Newtonian viscosity $\eta_s(0)$ [16, 17], our results for the tensile complex viscosity at various temperatures also fall onto a common curve when the angular frequency is scaled by $\eta^*(0)$ as shown in figure 10. We find that the entire master curve for $\eta^*(\omega)$ can be fitted reasonably well with the modified Maxwell equation:

$$\frac{\eta^*(\omega)}{\eta^*(0)} = \frac{1}{(1 + C\omega^2\tau^2)^{\beta'}} \qquad 0 < \beta' \leqslant 1 \tag{7}$$

where τ is a temperature-dependent relaxation time which we have set equal to $\tau(T) = \eta^*(0)(T)/E_\infty$ with E_∞ taken to be 6.63×10^{10} Pa as estimated from equation (3). We have included the shift parameter C in equation (7) in order to move the calculated curve along the abscissa since we have fixed τ as above. In a general fit, the parameter C can be incorporated into τ and only the two parameters τ and β' need to be determined. We find that the master curve for $\eta^*(\omega)$ can be fitted very well with $\beta' = 0.48$ and $C = 2.5$ as shown by the solid curve in figure 10.

For the Maxwell model having a single time constant, $\beta' = 0.5$ for the complex viscosity. At first glance, the fit to our data with $\beta' = 0.48$ would suggest that the distribution of relaxation times for the alloy is very narrow in contrast to the discussion in the previous sections. This, however, is a wrong interpretation. It is an error to compare the fitting parameter $\beta' = 0.48$

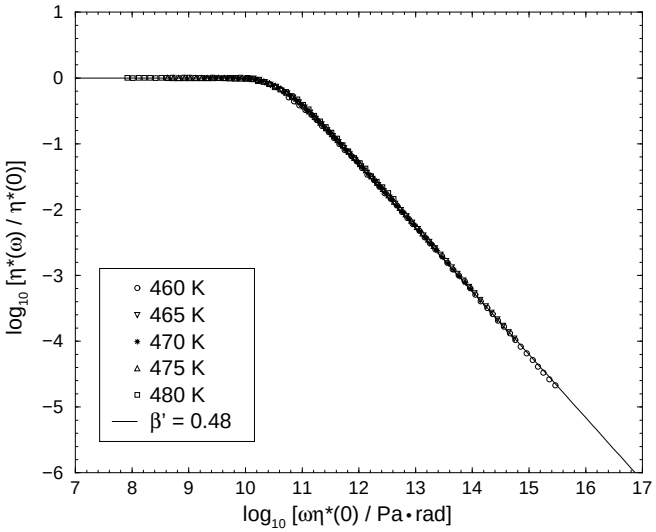

Figure 10. The master plot for the complex tensile viscosity curves when the angular frequency is scaled by $\eta^*(0)(T)$. The solid curve is the fit given by equation (7) with $C = 2.5$ and $\beta' = 0.48$.

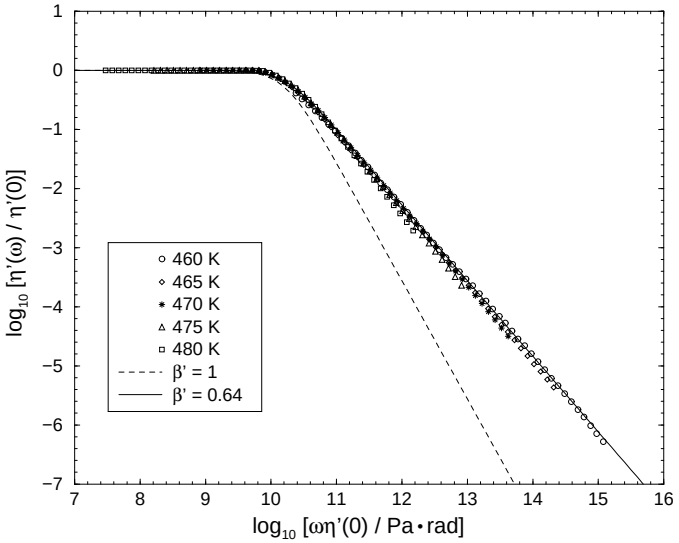

Figure 11. The master curve for the dynamic viscosity $\eta'(\omega)$ at different temperatures when the angular frequency is scaled by $\eta'(0)(T)$. The solid curve is the fit given by equation (7) with $C = 16.0$ and $\beta' = 0.64$. The dashed curve is the Maxwell relation with $C = 16.0$ and $\beta' = 1$.

with the Maxwell exponent for $\eta^*(\omega)$ because the zero-frequency value for the real, $\eta'(\omega)$, and imaginary, $\eta''(\omega)$, components of $\eta^*(\omega)$ are not equal for the alloy, as implied in figure 9, unlike the case for the Maxwell model. Only the experimental results for $\eta'(\omega)$ or $\eta''(\omega)$ can be compared directly with the Maxwell model.

In figure 11 we plot $\eta'(\omega)$ against angular frequency with both quantities scaled by $\eta'(0)(T)$. The data fall onto a master curve as for $\eta^*(\omega)$. We have used equation (7) with

$\eta^*(\omega)$ replaced by $\eta'(\omega)$ and $\eta^*(0)$ replaced by $\eta'(0)$ to fit the common curve. The parameters $C = 16.0$ and $\beta' = 0.64$ are found to provide a reasonably good fit to the data as shown by the solid curve in figure 11. In the case of the Maxwell model, $\beta' = 1$ for $\eta'(\omega)$ [21]. This is also shown by the dashed curve in figure 11. It is now quite clear that the master curve for the dynamic viscosity $\eta'(\omega)$ reflects a broad distribution of relaxation times rather than a single time constant.

4. Summary

We have presented dynamic measurements of the elastic and viscous components of the tensile modulus, and the complex and dynamic tensile viscosities, of $Pt_{60}Ni_{15}P_{25}$ over a 20 K interval below and close to the calorimetric glass transition temperature $T_g^c = 485 \pm 2$ K. From these data, three temperature-dependent relaxation times have been measured: (i) the position ω_{max} of the maximum in the loss peak of the tensile modulus, (ii) the limiting low-frequency value $\eta^*(0)$ of the complex tensile viscosity and (iii) the corresponding value $\eta'(0)$ for the dynamic viscosity. The three quantities have Arrhenius temperature dependences with approximately equal activation energies and indicate a change of relaxation times of approximately three orders of magnitude over the narrow temperature range. From the temperature dependences of ω_{max}, $\eta^*(0)$ and $\eta'(0)$, the supercooled $Pt_{60}Ni_{15}P_{25}$ alloy is shown to have an intermediate fragility strength with a fragility index of $m = 66 \pm 3$ at T_g^c or at T_g^v where the viscosity is 10^{12} Pa s.

The time–temperature superposition principle or thermorheological simplicity is found to apply for the storage and loss moduli, as well as the complex and dynamic viscosities, over the temperature interval investigated. Thermorheological simplicity has often been connected with Arrhenius temperature dependences of relaxation times [22]. Our results agree with this general trend. The resulting master curves after superposition reflect a broad distribution of intrinsic relaxation times. In order to obtain an estimate of the width of the distribution of timescales for the amorphous alloy, we have assumed that the master curve for the storage modulus arises from the superposition of exponentially decaying microscopic processes. The resulting discrete spectrum of relaxation times is very broad and asymmetric, being skewed towards higher frequencies. These are characteristic features of heterogeneous relaxation which have been observed previously for molecular and polymeric organic liquids [11–13]. It is found that approximately eight decades in the probability density of frequencies are required to reproduce the master curve for the storage modulus. Our results certainly indicate a very high degree of dynamic heterogeneity in the tensile relaxation process of the deeply supercooled $Pt_{60}Ni_{15}P_{25}$ alloy.

Acknowledgments

DNP gratefully acknowledges the receipt of a Science and Technology Agency (STA) Fellowship from the Japan Science and Technology Agency (JST).

References

[1] Laughlin W T and Uhlmann D R 1972 *J. Phys. Chem* **76** 2317
[2] Angell C A 1995 *Science* **267** 1924
[3] Böhmer R and Angell C A 1992 *Phys. Rev.* B **45** 10 091
[4] Böhmer R, Ngai K L, Angell C A and Plazek D J 1993 *J. Chem. Phys.* **99** 4201
[5] Liebermann H H (ed) 1993 *Rapidly Solidified Alloys* (New York: Dekker)

[6] Götze W and Sjögren L 1992 *Rep. Prog. Phys.* **55** 241
[7] A schematic diagram of the single-roller melt-spinning apparatus and a short description of the production procedure can be found at http://www.nrim.go.jp:8080/open/AP/Team/SingleRollerMeltSpin.html.
[8] Williams G and Watts D C 1970 *Trans. Faraday Soc.* **66** 80
Williams G, Watts D C, Dev S B and North A M 1971 *Trans. Faraday Soc.* **67** 1323
[9] Perera D N and Harrowell P 1998 *J. Non-Cryst. Solids* **235–237** 314
[10] Perera D N and Harrowell P 1998 *Phys. Rev. Lett.* **81** 120
[11] Böhmer R *et al* 1998 *J. Non-Cryst. Solids* **235–237** 1
[12] Tracht U, Heuer A and Spiess H W 1998 *J. Non-Cryst. Solids* **235–237** 27
[13] Richert R 1998 *J. Non-Cryst. Solids* **235-237** 41
[14] *Numerical Recipes* is freely available on-line at http://www.nr.com/.
[15] Ferry J D 1980 *Viscoelastic Properties of Polymers* (New York: Wiley) p 47
[16] Ferry J D 1980 *Viscoelastic Properties of Polymers* (New York: Wiley) pp 257–9, 516–8
[17] Kato H, Kawamura Y, Inoue A and Chen H S 1998 *Appl. Phys. Lett.* **73** 3665
[18] Graessley W W 1974 *Adv. Polym. Sci.* **16** 1
[19] Heyes D M, Kim J J, Montrose C J and Litovitz A 1980 *J. Chem. Phys.* **73** 3987
[20] Chen H S 1978 *J. Non-Cryst. Solids* **29** 223
[21] Ferry J D 1980 *Viscoelastic Properties of Polymers* (New York: Wiley) p 57
[22] Ngai K L 1987 *J. Non-Cryst. Solids* **95+96** 969
Ngai K L, Rendell R W and Plazek D J 1991 *J. Chem. Phys.* **94** 3018